



Novel radiomic analysis on bi-parametric MRI for characterizing differences between MR non-visible and visible clinically significant prostate cancer

Lin Li^{a,1}, Rakesh Shiradkar^{a,b,1}, Sree Harsha Tirumani^c, Leonardo Kayat Bittencourt^c, Pingfu Fu^d, Amr Mahran^e, Christina Buzzy^a, Phillip D. Stricker^f, Ardeshir R. Rastinehad^g, Cristina Magi-Galluzzi^h, Lee Ponsky^{e,i}, Eric Klein^j, Andrei S. Purysko^{j,k}, Anant Madabhushi^{b,1,*}

^a Center for Computational Imaging and Personalized Diagnostics, Case Western Reserve University, Cleveland, OH, USA

^b Department of Biomedical Engineering, Emory University and Georgia Institute of Technology

^c Department of Radiology, University Hospitals, Cleveland, OH, USA

^d Department of Population and Quantitative Health Sciences, Case Western Reserve University, Cleveland, OH, USA

^e Urology Institute, University Hospitals Cleveland Medical Center, Cleveland, OH, USA

^f Department of Urology, St. Vincent's Clinic, Sydney, NSW 2010, Australia

^g Department of Urology, Lenox Hill Hospital, Northwell Health, New York, NY, USA

^h Department of Pathology, University of Alabama at Birmingham, AL, USA

ⁱ Case Western Reserve University School of Medicine, Cleveland, OH, USA

^j Glickman Urological and Kidney Institute, Cleveland Clinic, Cleveland, OH, USA

^k Imaging Institute, Cleveland Clinic, Cleveland, OH, USA

¹ Atlanta Veterans Affairs Medical Center, Atlanta, GA, United States

ARTICLE INFO

Keywords:

Radiomic

Clinically significant prostate cancer

MR non-visible

ABSTRACT

Background: around one third of clinically significant prostate cancer (CsPCa) foci are reported to be MRI non-visible (MRI⁻).

Objective: To quantify the differences between MR visible (MRI⁺) and MRI⁻ CsPCa using intra- and peri-lesional radiomic features on bi-parametric MRI (bpMRI).

Methods: This retrospective and multi-institutional study comprised 164 patients with pre-biopsy 3T prostate multi-parametric MRI from 2014 to 2017. The MRI⁻ CsPCa referred to lesions with PI-RADS v2 score < 3 but ISUP grade group > 1. Three experienced radiologists were involved in annotating lesions and PI-RADS assignment. The validation set (D_v) comprised 52 patients from a single institution, the remaining 112 patients were used for training (D_t). 200 radiomic features were extracted from intra-lesional and peri-lesional regions on bpMRI.

Logistic regression with least absolute shrinkage and selection operator (LASSO) and 10-fold cross-validation was applied on D_t to identify radiomic features associated with MRI⁻ and MRI⁺ CsPCa to generate corresponding risk scores R^{MRI^-} and R^{MRI^+} . R_{bpMRI} was further generated by integrating R^{MRI^-} and R^{MRI^+} . Statistical significance was determined using the Wilcoxon signed-rank test.

Results: Both intra-lesional and peri-lesional bpMRI Haralick and CoLIAGe radiomic features were significantly associated with MRI⁻ CsPCa ($p < 0.05$). Intra-lesional ADC Haralick and CoLIAGe radiomic features were significantly different among MRI⁻ and MRI⁺ CsPCa ($p < 0.05$). R_{bpMRI} yielded the highest AUC of 0.82 (95 % CI 0.72–0.91) compared to AUCs of R^{MRI^+} 0.76 (95 % CI 0.63–0.89), and PI-RADS 0.58 (95 % CI 0.50–0.72) on D_v. R_{bpMRI} correctly reclassified 10 out of 14 MRI⁻ CsPCa on D_v.

* Correspondence to: Health Sciences Research Building II 1760 Haygood Drive, Suite N647Atlanta, 30322, Georgia.

E-mail address: anantm@emory.edu (A. Madabhushi).

¹ First authors.

Conclusion: Our preliminary results demonstrated that both intra-lesional and peri-lesional bpMRI radiomic features were significantly associated with MRI⁻ CsPCa. These features could assist in CsPCa identification on bpMRI.

1. Introduction

Prostate cancer (PCa) is one of the most common cancers among men in the US [1]. However, not all PCa patients require curative treatment [2]. Accurate identification of clinically significant prostate cancer (CsPCa) is critical to avoid under- or over-diagnosis. The CsPCa can be defined as the presence of International Society of Urological Pathology (ISUP) grade group > 1 (Gleason score 3 + 3 = 6) cancers with either a volume \geq 0.5 mL or extraprostatic extension [3].

Although multi-parametric magnetic resonance imaging (mpMRI) has played a critical role in PCa diagnosis, localization and risk stratification, biopsy is still assumed as the de-facto ground truth due to the chances of missing CsPCa on mpMRI [4,5]. Prostate Imaging-Reporting and Data System (PI-RADS) guidelines version 2.1 (v2.1) have been designed to standardize mpMRI interpretation for estimating the likelihood of a lesion being CsPCa [3]. Lesions assigned PI-RADS v2 score < 3 are deemed to have a low likelihood of being CsPCa and are potentially benign conditions or artifacts [3]. Studies have shown that mpMRI has a 76–94 % negative predictive value (NPV) for CsPCa detection at a patient level, when defining the MR-nonvisible as PI-RADS [3] or Likert [6] score < 3 and CsPCa as ISUP grade group > 1 [4,7–9]. However, PCa is often multifocal and more than one third of CsPCa foci have been reportedly missed by mpMRI [5]. Most studies have paid little attention to these CsPCa foci missed by mpMRI (MRI non-visible) and the public datasets have included few MRI non-visible CsPCa annotations for model training and validation [10,11]. Therefore, there is a need to investigate the characteristics of MRI non-visible CsPCa to assist with the improvement of detection accuracy of CsPCa on mpMRI.

Prostate bi-parametric magnetic resonance imaging (bpMRI) has demonstrated comparable performance to mpMRI for PCa diagnosis and characterization [12]. BpMRI comprises T2-weighted MRI (T2WI) and diffusion-weighted imaging (DWI) sequences, but excludes dynamic contrast-enhanced (DCE) imaging sequences due to its limited contribution to PCa diagnosis among treatment-naïve patients [12]. Preliminary studies have shown that bpMRI can be applied on biopsy naïve PCa patients to exclude CsPCa while reducing scan times and saving cost by avoiding contrast agent injection [13,14]. Additionally, the potential risk of long-term effects of gadolinium exposure and gadolinium-related anaphylaxis also motivate the application of bpMRI for PCa diagnosis [14].

Radiomic analysis involves the quantitative extraction of sub-visual features on radiological imaging in a high-throughput manner [15, 16]. These radiomic features are the values calculated through pre-defined mathematical equations on image intensities among regions of interest and these features can be used as inputs to train machine learning models for clinical applications [17]. Radiomic analysis is also being widely explored on prostate bpMRI to quantify underlying characteristics of PCa, e.g., shape, and texture [18,19]. Previous studies have suggested that radiomic features extracted from the adjacent regions of lesions on bpMRI could aid in assessing disease aggressiveness [18,20]. For example, Algohary and et al. showed that radiomic features extracted from the lesion adjacent regions on bpMRI can assist in identifying CsPCa where PI-RADS and biopsy results were discordant [18]. Recently, Houlahan and et al. observed that hallmarks of nimbus, an aggressive micro-environmental and pathological phenomenon of prostate cancer, were associated with MRI visibility of PCa [21]. These findings suggested the need to explore radiomic features extracted not only within the lesions (intra-lesion) but also from corresponding adjacent regions (peri-lesion) in identifying MRI non-visible CsPCa.

In this multi-institutional study, we focused on investigating the

association between both intra- and peri-lesional radiomic features with CsPCa MRI visibility on bpMRI. To the best of our knowledge, this is the first study with the largest multi-institutional dataset, dedicated to addressing the question of whether radiomic analysis could help better identify the phenotype of MRI non-visible CsPCa on bpMRI.

2. Materials and methods

2.1. Ethics statement

This retrospective study was approved by the Case Western Reserve University, University Hospitals, and Cleveland Clinic Institutional Review Board (IRB), and is compliant with the Health Insurance Portability and Accountability Act (HIPAA); de-identified data was used, and no protected health information was needed. The need for informed consent from all patients was waived by the IRB.

2.2. Patient selection

The patient selection criteria adopted by this study were as shown in Fig. 1. A total of 164 PCa patients from four institutions were finally identified. N = 52 patients from a single institution were assigned as the validation set (D_v) and the remaining patients comprised of the training set (D_t , N = 112). The non-visible (MRI⁻) lesions on bpMRI referred to lesions with PI-RADS < 3 and visible (MRI⁺) lesions with PI-RADS \geq 3. MRI⁻ CsPCa were defined as PCa with PI-RADS < 3 but ISUP grade group > 1.

2.3. MRI protocol

The mpMRI were collected on 3T scanners with either a surface pelvic phased-array coil (PPAC) or an endorectal coil (ERC) with acquisition parameters presented in Supp. Table 1. The apparent diffusion coefficient (ADC) maps were generated from DWI data using the corresponding scanner software at each institution.

2.4. Annotation delineation

Radiologists initially annotated suspicious lesions on bpMRI using the 3D Slicer software [22] while being blinded to the lesion diagnosis on pathology. Next, they referred to pathology either from MRI-targeted and systematic biopsy or surgical specimens to include the CsPCa foci which were missed initially. Specifically, when surgical specimens were available, they were spatially co-registered to bpMRI to map the lesion annotations onto bpMRI [23]. The co-registered annotations were then compared with manual annotations and refined by radiologists using the 3D Slicer software. Our cohort also comprised delineations of prostatitis and normal tissue regions [24,25] with reference to the surgical specimen which were included as negative control cases. When only biopsy location information was available, the CsPCa regions were delineated based off visual inspection.

After a wash-out time interval of at least two months, the lesion annotations were viewed and assigned PI-RADS V2.1 scores in a way that was blinded to their clinical diagnosis by experienced board-certified genitourinary radiologists (A.S.P, 10 years of experience, S.H.T, 7 years of experience; and L.K.B 10 years of experience) using the RadiAnt DICOM Viewer [26]. The lesion adjacent regions were estimated by expanding the boundary of lesions by 3 mm while clipping the region outside of the prostate.

In addition, to explore the morphologic basis of the radiomic features

identified to be associated with MRI- CsPCa, N = 34 radical prostatectomy (RP) patients were collected for quantitative tissue composition analysis. The prostate specimens were firstly sliced into quadrants, hematoxylin and eosin (H&E) stained and reviewed by an experienced pathologist. The pathologist identified N = 50 lesions, generated RP

maps illustrating the spatial location of these lesions. The pathologist and radiologist consensually provided spatial correspondences between MRI and RP slices. The H&E stained slices were digitized at 20 ×, with cancer lesions annotated by the pathologist, and were then spatially co-registered with T2WI via a multi-scale deformable registration method

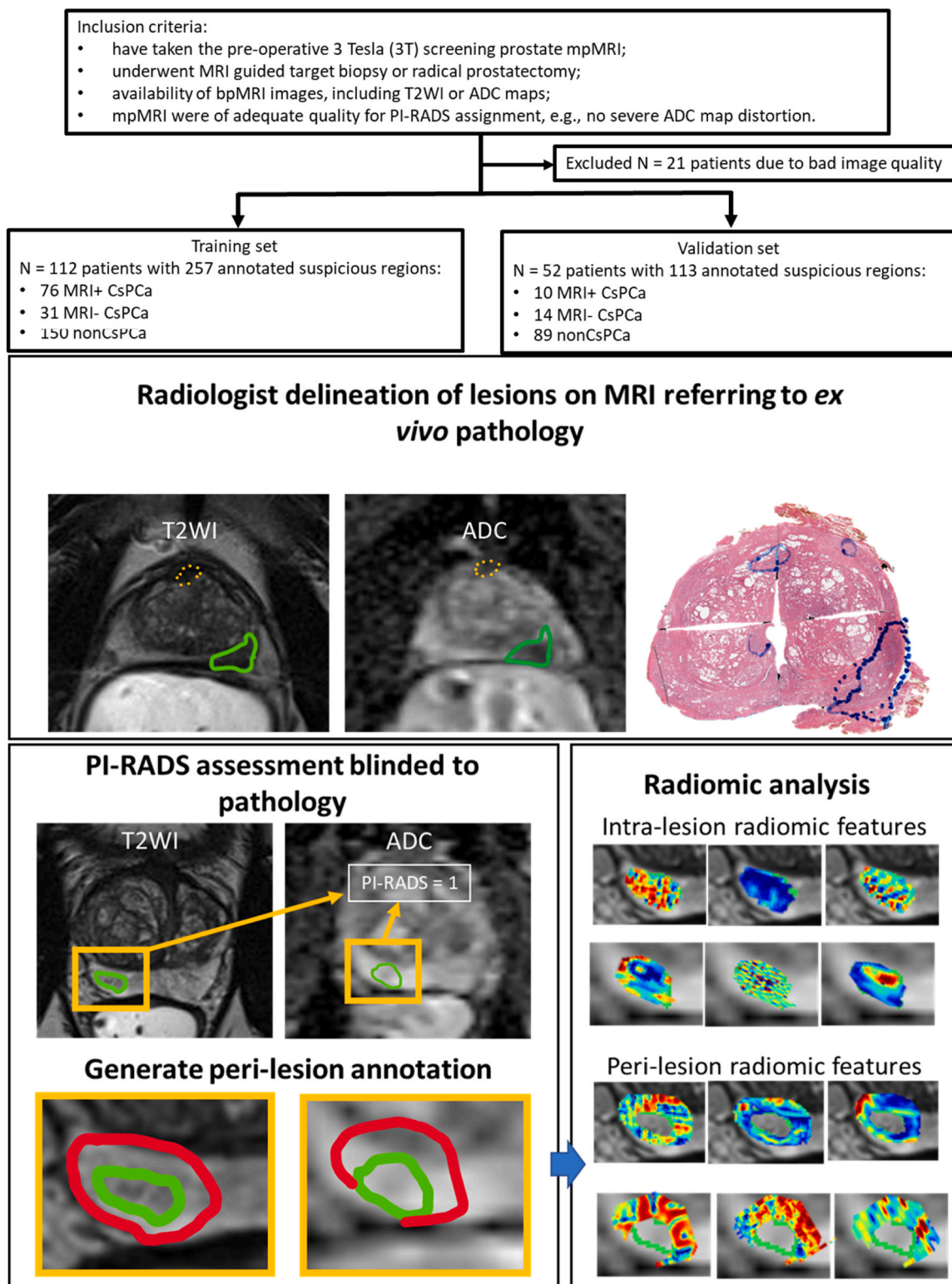


Fig. 1. Flowchart illustrating patient selection criteria and an overview of the experimental design used in this study. Radiologists initially delineated suspicious lesions (green outline) on bpMRI blinded to pathologic diagnosis. They then referred to pathology (either systematic biopsy or surgical specimen) to update their delineations (orange dotted outline). PI-RADS scores were assigned by radiologists to the delineated lesions blinded to pathologic diagnosis following a wash-out period. The red outline indicates peri-lesional region (derived as 3 mm annular ring outside the lesion boundary (green)) retained within the prostate boundary.

[23]. This maps lesion annotations on to MRI, which were then reviewed by the radiologist and edited as necessary.

2.5. MRI pre-processing and radiomic analysis

Due to the multi-institutional nature of this study, a nonparametric intensity standardization method [27] was used to alleviate the heterogeneity of T2WI intensity distributions across scans. Furthermore, we employed a previously published method to estimate the bias field introduced by ERC coil and subtract it from the acquired MRI data [28]. In addition, both T2WI and ADC maps were resampled at the same spatial resolution in the axial plane (0.5 × 0.5 mm).

After pre-processing, 200 2D radiomic features were extracted from the axial plane within intra- and peri-lesional regions on both T2WI and ADC maps, including first and second order statistics, Gabor [29], Laws [30], Haralick [31] and CoLIAGe [32] features. These features have been previously identified for PCa characterization [18,19]. Statistics including mean, standard deviation, skewness, and kurtosis were calculated for each radiomic feature to characterize its distribution within each lesion and adjacent regions.

2.6. Statistical analysis

First, radiomic features were identified to distinguish CsPCA lesions and normal tissue regions using Wilcoxon signed-rank test. Then, top radiomic features (F_{T2WI}^{MRI-} , F_{T2WI}^{MRI+} , F_{ADC}^{MRI-} and F_{ADC}^{MRI+}), which were associated with MRI⁻ or MRI⁺ CsPCA, were identified using the least absolute shrinkage and selection operator (LASSO) [33] with logistic regression in D_t . The odds ratios (ORs) were calculated via multivariate analysis to evaluate the contribution of each selected radiomic feature. In addition, Wilcoxon signed-rank test was used to identify radiomic features that were significantly different between MRI⁺ and MRI⁻ CsPCA. Then, Spearman correlation analysis was applied to evaluate the association between these radiomic features and the pathological characteristics of CsPCA on a subset of cases where surgical specimens were available.

Subsequently a generalized linear mixed-effect models were adopted to train lesion-wise machine learning classifiers to account for random variability introduced when multiple lesions were collected from the same patient. Classifiers C_{T2WI}^{MRI-} , C_{T2WI}^{MRI+} , C_{ADC}^{MRI-} , and C_{ADC}^{MRI+} , were trained with 10-fold cross-validation to predict lesions as CsPCA using F_{T2WI}^{MRI-} , F_{T2WI}^{MRI+} , F_{ADC}^{MRI-} , and F_{ADC}^{MRI+} , respectively, and producing radiomic risk scores R_{T2WI}^{MRI-} , R_{T2WI}^{MRI+} , R_{ADC}^{MRI-} , and R_{ADC}^{MRI+} respectively. F_{T2WI}^{MRI-} , F_{T2WI}^{MRI+} , F_{ADC}^{MRI-} and F_{ADC}^{MRI+} were integrated to train classifiers, C_{T2WI} and C_{ADC} , producing risk score R_{T2WI} and R_{ADC} . Finally, R_{T2WI} and R_{ADC} were ensemble to generate R_{bpMRI} , the ensembling approach involved selecting the greater of the risk scores from R_{T2WI} and R_{ADC} for each lesion. The classifiers and the risk scores were both constructed using the rms and glmnet packages in R software version 3.6.

The contribution of radiomic risk scores in predicting CsPCA were further evaluated using multivariate analysis and decision curve analysis. Furthermore, area under receiver operating characteristic curve (AUC), sensitivity, specificity, NPV and positive predictive value (PPV) were calculated to evaluate the classification performance of radiomic risk scores.

3. Results

3.1. Demographic and clinical characteristics

Demographic and clinical characteristics of all 164 patients are illustrated in Table 1. 34 % (45/131) CsPCA were assigned PI-RADS < 3, which correspond to 29 % (31/107) and 58 % (14/24) of our training and validation cohorts respectively. In addition, we had N = 73 patients with n = 150 lesions in D_t read by two experienced radiologists. The Cohen's kappa of PI-RADS scores was found to be 0.71 between the two

Table 1

Demographic and disease characteristics of all 164 patients. PSA = prostate specific antigen; SD = standard deviation; ISUP = International Society of Urological Pathology; * indicates statistically significant difference.

	D_t	D_v
# Patients	112	52
# lesions	257	113
Median age (range)	65 (40–88)	63 (43–81)
Mean pretreatment PSA ± SD, ng/mL (range)	8.08 ± 6.14 (1.2–38.6)	5.77 ± 4.15 (2.3–25)
Pathologic ISUP grade, n/# ROI (%)		
0	105/257(40.70)	73/113 (64.60)
1	46/257(17.83)	16/113 (14.16)
2	63/257(24.42)	17/113 (15.04)
3	28/257(10.85)	0/113 (0.00)
4	13/257(5.04)	0/113 (0.00)
5	3/257(1.16)	7/113 (6.19)
PI-RADS v2, n/# lesions (%)		
1	20/257(7.75)	52/113 (46.02)
2	126/257(48.84)	34/113 (30.09)
3	21/257(8.14)	3/113 (2.65)
4	49/257(18.99)	21/113 (18.58)
5	41/257(15.89)	3/113 (2.65)

radiologists. A stronger agreement (kappa = 0.81) was reached between the two readers for PI-RADS lesions with a cut-off of PI-RADS 3.

3.2. Identify T2WI and ADC radiomic features that are associated with MRI⁻ CsPCA

Table 2 lists radiomic features F_{T2WI}^{MRI-} and F_{ADC}^{MRI-} that were found to be associated with MRI⁻ CsPCA. Features labeled with asterisk in Table 2 were independently associated with CsPCA on D_v via multivariate analysis ($p < 0.05$). It was observed that the peri-lesional bpMRI radiomic features labeled with asterisk all have odds ratios greater than 1. In addition, F_{T2WI}^{MRI+} and F_{ADC}^{MRI+} that were found to be associated with MRI⁺ CsPCA are listed in Supp. Table 2.

N = 9 intra-lesional and N = 4 peri-lesional radiomic features, specifically Haralick [31] and CoLIAGe [32] features derived from T2WI and ADC maps, showed significant differences between MRI⁺ and MRI⁻ CsPCA (Supp. Table 3). Furthermore, to explore the morphologic basis of the radiomic features identified to be associated with MRI⁻ CsPCA, we identified 34 patients who underwent RP and had digitized H&E stained surgical specimens of sufficient quality for quantitative tissue composition analysis. Compartments of tumor tissue, including gland lumen, epithelial tissue, and stroma, on the surgical specimens were segmented using the Unet segmentation network [34] at 10 × resolution. Spearman's correlations between the prostate tissue composition and identified features were calculated with Benjamini-Hochberg correction [35]. The statistical significance of the correlation coefficients was defined as a false discovery rate ≤ 0.2 [35]. The lumen area was found to be negatively correlated with the standard deviation of intra-lesion ADC Haralick features, while adjusting the correlation coefficient to − 0.34. It was observed that MRI⁻ CsPCA lesions had less heterogeneous intra-lesion ADC Haralick feature expression and tended to have larger lumen area compared to MRI⁺ CsPCA lesions. (Fig. 2)

3.3. Investigating association of radiomic risk scores with CsPCA

Our final model contained 32 radiomic features (22 intra- and 10 peri-tumoral features). Table 3 lists the AUC, sensitivity, specificity, NPV and PPV results of R_{T2WI} , R_{ADC} , R_{bpMRI} and PI-RADS scores on D_v . In addition, the classification performance of the radiomic risk score, R_{bpMRI}^{MRI+} , which was ensemble using R_{T2WI}^{MRI+} and R_{ADC}^{MRI+} , were also measured to evaluate the contribution of R_{T2WI}^{MRI-} and R_{ADC}^{MRI-} in identifying CsPCA. R_{T2WI}^{intra} is the radiomic risk score that only combines the intra-tumoral radiomic features.

Table 2
Identified intra- and peri-lesion radiomic features associated with MRI⁻ CsPCa. In addition, tumor size was evaluated for its association to CsPCa. * indicates a statistically independent factor for CsPCa.

Feature type	Feature name	Statistics	region	Odds ratio	Feature number	
<i>F^{MRI⁻}_{T2WI}</i>	Haralick Information measure of correlation 2	Standard deviation	Intra-lesion	1.43	3	
	CoLIAGe Information measure of correlation 1*	skewness	Intra-lesion	0.98		
	Haralick Sum Entropy Laws 6	kurtosis	Intra-lesion	1.07		
	<i>F^{MRI⁻}_{ADC}</i>	Haralick Information measure of correlation 2	Standard deviation	Peri-lesion	1.01	13
		Haralick Correlation	Standard deviation	Peri-lesion	1.43	
		Haralick Correlation*	Standard deviation	Peri-lesion	0.88	
		Haralick Entropy	Skewness	Peri-lesion	1.97	
		Haralick Sum Average	Skewness	Peri-lesion	1.15	
		CoLIAGe Information measure of correlation 2*	Skewness	Peri-lesion	1.31	
		CoLIAGe Difference Variance	Skewness	Peri-lesion	1.19	
		CoLIAGe Information measure of correlation 1	Skewness	Peri-lesion	1.19	
		CoLIAGe Information measure of correlation 1 Laws 6	Skewness	Peri-lesion	0.98	
		Haralick Inverse Difference Moment	Kurtosis	Peri-lesion	1.20	
		Haralick Information measure of correlation 1	Kurtosis	Peri-lesion	0.87	
		CoLIAGe Sum Average	Kurtosis	Peri-lesion	1.50	
		CoLIAGe Correlation	mean	Intra-lesion	0.96	
		CoLIAGe Information measure of correlation 1	mean	Intra-lesion	0.82	
		Haralick information measure of correlation 1	Standard deviation	Intra-lesion	0.90	
		CoLIAGe Information measure of correlation 1*	Standard deviation	Intra-lesion	1.13	
Tumor size	Haralick Information measure of correlation 1	Standard deviation	Peri-lesion	1.29	2	
	CoLIAGe Correlation	Standard deviation	Intra-lesion	1.42		
	Haralick Information measure of correlation 1	Standard deviation	Peri-lesion	1.77		
	CoLIAGe Inverse Difference Moment *	Standard deviation	Peri-lesion	2.03		
	Tumor size	NA	Intra-lesion	1.0		

We found that R_{bpMRI} yielded the highest AUC of 0.82 and correctly reclassified 10 out of 14 MRI⁻ CsPCa on D_v at the optimal cut-off point learned on D_t . In addition, the multivariate analysis demonstrated that R_{bpMRI} was independent compared to R_{bpMRI}^{MRI+} , in terms of association with CsPCa (p-value < 0.05). Decision curve analysis (Fig. 3) indicated that the R_{bpMRI} produced larger net-benefit in identifying CsPCa compared to PI-RADS score and R_{bpMRI}^{MRI+} .

4. Discussion

In this multi-institutional study, we sought to evaluate whether radiomic analysis on bpMRI could enable identification of subvisual image features associated with CsPCa MRI visibility. Specifically, we sought to evaluate whether radiomic analysis of peri-lesional regions could allow for better MRI⁻ CsPCa characterization by capturing features of the tumor microenvironment.

Although PI-RADS tends to be influenced by inter-reader variability [36], our study revealed a moderate inter-reader reliability (kappa = 0.71) between two experienced radiologists and a strong agreement (kappa = 0.81) when using PI-RADS ≥ 3 as the cut-off [37]. Our findings suggest that the PI-RADS based threshold could potentially be an appropriate cut off for definition of MRI⁻ CsPCa, as used this study.

We observed that intra- and peri-lesional bpMRI Haralick and CoLIAGe features were significant predictors of MRI⁻ CsPCa (Table 2). The odds ratios of the identified peri-lesional bpMRI radiomic features indicate that peri-lesional area of MRI⁻ CsPCa tended to have more heterogeneous texture, as captured by Haralick and CoLIAGe features on bpMRI compared to non-CsPCa lesions. A number of studies have investigated computer-aided systems for CsPCa detection on mpMRI using radiomic or deep learning models [18,20,38]. However, most of these studies only included MRI⁺ CsPCa lesions in the training data [18, 20], without focusing on the characteristics of MRI⁻ CsPCa. For example, Algohary and et al. showed that bpMRI radiomic features can aid in identifying CsPCa in highly challenging cases where the PI-RADS and biopsy results were discordant [18]. However, in their study, no MRI⁻ CsPCa were included in the training set. Hiremath and et al. integrated deep learning-based bpMRI predictors with PI-RADS score and clinical parameters for CsPCa classification, yielding an AUC = 0.76 [20]. However, their study did not discuss how the deep learning-based predictors contribute to identifying MRI⁻ CsPCa.

Recently, some studies attempted to establish correlation between MRI and histopathology to explore a deeper understanding of PCA characterization [25]. Our study also attempted to explore radiomic and histopathological correlations between MRI⁺ and MRI⁻ CsPCa. Our results indicated a majority of significant radiomic features (Supp. Table 3) were mostly derived from ADC maps suggesting that MRI⁺ CsPCa tended to be more heterogenous on ADC maps compared to non-visible CsPCa. In addition, the gland lumen of MRI⁻ CsPCa was observed to be larger and more loosely distributed within tumor regions compared to MRI⁺ CsPCa. Meanwhile, the gland lumen composition ratio was also found to be negatively associated with the intra-lesion ADC Haralick features (Fig. 2). This finding appears to suggest that gland lumen area and distribution impact CsPCa MRI visibility and that intra-lesion ADC Haralick features may be associated with this histopathological signature. Previous studies have also corroborated the fact that histopathological difference exists between MRI⁺ and MRI⁻ PCA [39]. For example, a previous study by van Houdt and et al. demonstrated that MRI⁻ PCA had lower tumor density and heterogeneous tumor morphology compared to MRI⁺ PCA [39].

Furthermore, on multivariate analysis we observed that the radiomic risk score R_{bpMRI} derived from both MRI⁺ and MRI⁻ CsPCa associated radiomic features yielded independent value to R_{bpMRI}^{MRI+} and PI-RADS score for CsPCa classification on bpMRI. The decision curve analysis illustrated that the net-benefit of R_{bpMRI} is superior to PI-RADS or R_{bpMRI}^{MRI+}

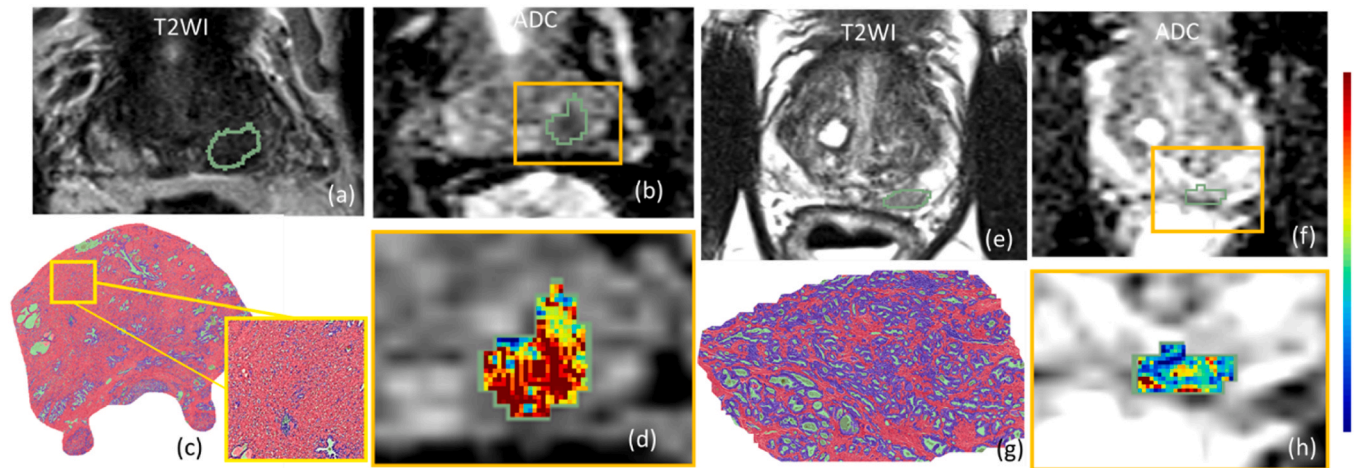


Fig. 2. Visualization of radiomic features and corresponding pathologic characteristics of MRI⁺ and MRI⁻ CspCa. (a)–(d) is an example of a patient with MRI⁺ CspCa. PI-RADS = 5, ISUP group = 2. (a) T2WI with PCa annotated (green line); (b) ADC map with PCa annotated (green line); (c) corresponding PCa tissue cropped from H&E stained surgical specimens with segmented lumen (green), epithelium (purple) and stroma (pink) highlighted; (d) a Haralick feature derived on ADC maps; (e)–(h) is an example of MRI⁻ CspCa. PI-RADS = 2 and ISUP group = 2.

Table 3

AUC, sensitivity, specificity, balanced accuracy, NPV and PPV results on D_v using the radiomic risk score.

Classifiers	AUC	Sen.	Spec.	Balanced Acc.	NPV	PPV	TP	TN	FP	FN
R_{T2WI}	0.75 (0.62–0.88)	0.75	0.56	0.655	0.89	0.32	18	50	39	6
R_{ADC}	0.73 (0.62–0.84)	0.50	0.80	0.650	0.85	0.40	12	71	18	12
R_{bpMRI}	0.82 (0.72–0.91)	0.83	0.55	0.690	0.92	0.33	20	49	40	4
R_{bpMRI}^{MRI+}	0.76 (0.63–0.89)	0.58	0.79	0.685	0.88	0.42	14	70	19	10
R_{bpMRI}^{intra}	0.65 (0.51–0.79)	0.54	0.78	0.660	0.85	0.29	14	55	34	10
PI-RADS	0.58 (0.50–0.72)	0.42	0.81	0.615	0.84	0.37	10	72	17	14

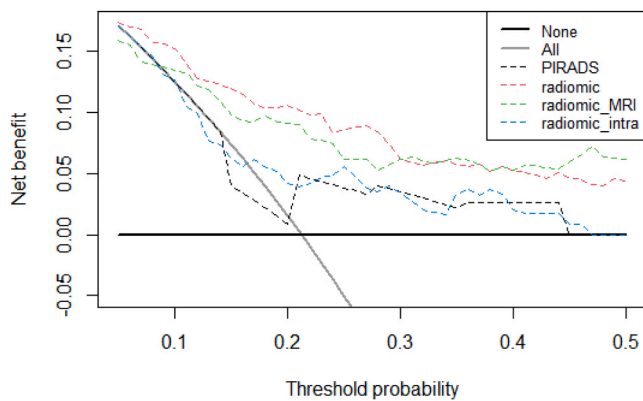


Fig. 3. The net-benefit plot for PI-RADS score (black), R_{bpMRI} (red), R_{bpMRI}^{MRI+} (green) and R_{T2WI}^{intra} (blue).

when assuming that the occurrence of CspCa for biopsy-naïve patients with elevated PSA is 30 % or less (Fig. 3). Meanwhile, the prevalence of CspCa for biopsy-naïve patients with elevated PSA was observed less than 30 % [40]. Therefore, these results suggest statistically significant contributions of MRI⁻ CspCa associated radiomic features in identifying MRI⁻ CspCa on bpMRI.

Our study was limited by a relatively small number of patients (n = 164), though it is worth noting that the sample size was

comparable to other recent studies that have employed radiomic analysis for prostate cancer [18,41,42]. Another limitation was the fact that the study was completely retrospective in nature, additional multi-site prospective validation is warranted. Manual delineation of the lesions was performed by expert radiologists, however, we do acknowledge that annotation by different experts can introduce bias and variability in target definition [43].

In conclusion, this study identified both intra- and peri-lesional bpMRI radiomic features that were significantly associated with MRI⁻ CspCa. Our study revealed that MRI⁻ CspCa tend to have a more heterogeneous texture in the peri-lesional region compared to non-CspCa lesions on bpMRI. In addition, we constructed a radiomic risk score that integrated MRI⁺ and MRI⁻ CspCa associated radiomics features for CspCa identification. With additional validation, this radiomics risk score could potentially serve as a decision support tool to aid clinicians in better identification and risk stratification of both visible and non-visible prostate lesions on bpMRI.

CRedit authorship contribution statement

Lin Li, Rakesh Shiradkar and Anant Madabhushi conceived the study, designed the study, supervised the study, and interpreted the results. Lin Li, Rakesh Shiradkar, Sree Harsha Tirumani, Leonardo Kayat Bittencourt, Amr Mahran, Christina Buzzy, Phillip D. Stricker, Cristina Magi-Galluzzi, Lee Ponsky, Eric Klein and Andrei S. Purysko collected the data. Lin Li and Rakesh Shiradkar drafted the manuscript. Lin Li and Rakesh Shiradkar contributed equally and were the co-first authors. Lin

Li, Rakesh Shiradkar, Pingfu Fu, Christina Buzzy and Anant Madabhushi provided critical revision of the manuscript for important intellectual content. Lin Li and Pingfu Fu contributed to the statistical analysis. Anant Madabhushi and Rakesh Shiradkar obtained fundings.

Conception and design: Lin Li, Rakesh Shiradkar, Anant Madabhushi. Acquisition of data: Lin Li, Rakesh Shiradkar, Sree Harsha Tirumani, Leonardo Kayat Bittencourt, Amr Mahran, Christina Buzzy, Phillip D. Stricker, Cristina Magi-Galluzzi, Lee Ponsky, Eric Klein, Andrei S. Purysko. Analysis and interpretation of data: Lin Li. Drafting of the manuscript: Lin Li, Rakesh Shiradkar. Critical revision of the manuscript for important intellectual content: Lin Li, Rakesh Shiradkar. Statistical analysis: Lin Li, Pingfu Fu. obtaining funding: Anant Madabhushi, Rakesh Shiradkar. administrative, technical, or. material support: Christina Buzzy. supervision: Anant Madabhushi.

Lee Ponsky: Writing – review & editing, Data curation. **Eric Klein:** Writing – review & editing, Data curation. **Lin Li:** Writing – review & editing, Writing – original draft, Visualization, Validation, Project administration, Methodology, Investigation, Data curation, Conceptualization. **Leonardo Kayat Bittencourt:** Writing – review & editing, Data curation. **Pingfu Fu:** Writing – review & editing, Methodology. **Andrei S. Purysko:** Writing – review & editing, Data curation. **Rakesh Shiradkar:** Writing – review & editing, Writing – original draft, Validation, Methodology, Funding acquisition, Conceptualization. **Anant Madabhushi:** Writing – review & editing, Supervision, Funding acquisition, Conceptualization. **Sree Harsha Tirumani:** Writing – review & editing, Data curation. **Phillip D. Stricker:** Writing – review & editing, Data curation. **Ardeshir R Rastinehad:** Writing – review & editing, Data curation. **Amr Mahran:** Writing – review & editing, Data curation. **Christina Buzzy:** Writing – review & editing, Data curation. **Cristina Magi-Galluzzi:** Writing – review & editing, Data curation.

Ethics statement

This retrospective study was approved by the Case Western Reserve University, University Hospitals, and Cleveland Clinic Institutional Review Board (IRB), and is compliant with the Health Insurance Portability and Accountability Act (HIPAA); de-identified data was used, and no protected health information was needed. The need for informed consent from all patients was waived by the IRB.

Funding

Research reported in this publication was supported by the National Institutes of Health National Cancer Institute under R01CA208236-01A1 and the United State Department of Defense Congressionally Directed Medical Research Programs under W81XWH-18-10-524 and W81XWH-20-1-0851.

The content is solely the responsibility of the authors and does not necessarily represent the official views of the National Institutes of Health, the Department of Defense, or the United States Government.

Declaration of Competing Interest

The authors declare the following financial interests/personal relationships which may be considered as potential competing interests: Anant Madabhushi reports a relationship with Picture Health that includes: consulting or advisory and equity or stocks. Anant Madabhushi reports a relationship with Elucid Bioimaging that includes: equity or stocks. Anant Madabhushi reports a relationship with Inspirata Inc that includes: equity or stocks. Anant Madabhushi reports a relationship with Aiforia Inc that includes: consulting or advisory. Anant Madabhushi reports a relationship with SimBioSys Inc that includes: consulting or advisory. Anant Madabhushi reports a relationship with Biohme that includes: consulting or advisory. Anant Madabhushi reports a relationship with Castle Biosciences Inc that includes: consulting or advisory. Anant Madabhushi reports a relationship with AstraZeneca that

includes: funding grants. Anant Madabhushi reports a relationship with Boehringer Ingelheim Pharmaceuticals Inc that includes: funding grants. Anant Madabhushi reports a relationship with Eli Lilly and Company that includes: funding grants. Anant Madabhushi reports a relationship with Bristol Myers Squibb Co that includes: funding grants. Andrei S Purysko reports a relationship with American College of Radiology that includes: funding grants. Andrei S Purysko reports a relationship with Blue Earth Diagnostics that includes: consulting or advisory, funding grants, and travel reimbursement. Andrei S Purysko reports a relationship with University of Missouri that includes: consulting or advisory. Andrei S Purysko reports a relationship with Koelis that includes: consulting or advisory. Andrei S Purysko reports a relationship with Profound Medical that includes: travel reimbursement. Sree Harsha Tirumani reports a relationship with Radiological Society of North America that includes: funding grants. Andrei S Purysko has patent #Radiomic features of prostate bi-parametric magnetic resonance imaging (BPMRI) associate with decipher score Patent number: 11017896 issued to UNIV CASE WESTERN RESERVE (US) CLEVELAND CLINIC FOUND (US). Anant Madabhushi has patent #US9235887B2 issued to Boston University Rutgers State University of New Jersey University of Pennsylvania Penn Elucid Bioimaging Inc.

Data sharing statement

Data generated or analyzed during the study are available from the corresponding author by request.

Acknowledgments

Research reported in this publication was supported by the National Institutes of Health National Cancer Institute under R01CA208236-01A1 and the United State Department of Defense Congressionally Directed Medical Research Programs under W81XWH-18-10-524 and W81XWH-20-1-0851.

The content is solely the responsibility of the authors and does not necessarily represent the official views of the National Institutes of Health, the Department of Defense, or the United States Government.

Appendix A. Supporting information

Supplementary data associated with this article can be found in the online version at [doi:10.1016/j.ejro.2023.100496](https://doi.org/10.1016/j.ejro.2023.100496).

References

- [1] Key Statistics for Prostate Cancer | Prostate Cancer Facts. (<https://www.cancer.org/cancer/prostate-cancer/about/key-statistics.html>). (Accessed 14 April 2022).
- [2] N.C.C.N. Clinical, Practice guidelines in oncology, Prostate Cancer Version 2 (2022).
- [3] PI-RADS. (<https://www.acr.org/Clinical-Resources/Reporting-and-Data-Systems/PI-RADS>).
- [4] H.U. Ahmed, et al., Diagnostic accuracy of multi-parametric MRI and TRUS biopsy in prostate cancer (PROMIS): a paired validating confirmatory study, *Lancet* 389 (2017) 815–822.
- [5] D.C. Johnson, et al., Detection of individual prostate cancer foci via multiparametric magnetic resonance imaging, *Eur. Urol.* 75 (2019) 712–720.
- [6] A.B. Rosenkrantz, et al., Comparison of interreader reproducibility of the prostate imaging reporting and data system and likert scales for evaluation of multiparametric prostate MRI, *Am. J. Roentgenol.* 201 (2013) W612–W618.
- [7] N.J. Sathianathan, et al., Negative predictive value of multiparametric magnetic resonance imaging in the detection of clinically significant prostate cancer in the prostate imaging reporting and data system era: a systematic review and meta-analysis, *Eur. Urol.* 78 (2020) 402–414.
- [8] A.G. Wibmer, et al., MRI-detectability of clinically significant prostate cancer relates to oncologic outcomes after prostatectomy, *Clin. Genitourin. Cancer* (2022), <https://doi.org/10.1016/j.clgc.2022.04.001>.
- [9] J.M. Norris, et al., What type of prostate cancer is systematically overlooked by multiparametric magnetic resonance imaging? An analysis from the PROMIS cohort, *Eur. Urol.* 78 (2020) 163–170.
- [10] L. Geert Litjens, D. Oscar, B. Jelle, K. Nico, H. Henkjan, ProstateX Challenge data, 2017. At (<https://doi.org/10.7937/K9TCLIA.2017.MUR55CL>).

- [11] The PI-CAI Challenge – Grand Challenge. (grand-challenge.org) (<https://pi-cai.grand-challenge.org/>).
- [12] S. Woo, et al., Head-to-head comparison between biparametric and multiparametric MRI for the diagnosis of prostate cancer: a systematic review and meta-analysis, *Am. J. Roentgenol.* 211 (2018) W226–W241.
- [13] B. Israël, et al., Multiparametric magnetic resonance imaging for the detection of clinically significant prostate cancer: what urologists need to know. Part 2: interpretation, *Eur. Urol.* 77 (2020) 469–480.
- [14] E.J. Bass, et al., A systematic review and meta-analysis of the diagnostic accuracy of biparametric prostate MRI for prostate cancer in men at risk, *Prostate Cancer Prostatic Dis.* 24 (2021) 596–611.
- [15] R.J. Gillies, P.E. Kinahan, H. Hricak, Radiomics: images are more than pictures, they are data, *Radiology* 278 (2015) 563–577.
- [16] D. Bonekamp, et al., Radiomic machine learning for characterization of prostate lesions with MRI: comparison to ADC values, *Radiology* 289 (2018) 128–137.
- [17] F. Coppola, et al., Human, all too human? An all-around appraisal of the “artificial intelligence revolution” in medical imaging, *Front. Psychol.* 12 (2021).
- [18] A. Algohary, et al., Combination of peri-tumoral and intra-tumoral radiomic features on bi-parametric MRI accurately stratifies prostate cancer risk: a multi-site study, *Cancers* 12 (2020) 2200.
- [19] L. Li, et al., A novel imaging based Nomogram for predicting post-surgical biochemical recurrence and adverse pathology of prostate cancer from pre-operative bi-parametric MRI, *EBioMedicine* 63 (2021).
- [20] A. Hiremath, et al., An integrated nomogram combining deep learning, Prostate Imaging–Reporting and Data System (PI-RADS) scoring, and clinical variables for identification of clinically significant prostate cancer on biparametric MRI: a retrospective multicentre study, *Lancet Digit. Health* 3 (2021) e445–e454.
- [21] K.E. Houlihan, et al., Molecular hallmarks of multiparametric magnetic resonance imaging visibility in prostate cancer, *Eur. Urol.* (2019).
- [22] S. Pieper, M. Halle, R. Kikinis, 3D slicer, in: *Proceedings of the 2004 2nd IEEE International Symposium on Biomedical Imaging: Nano to Macro (IEEE Cat No. 04EX821)*, vol. 1, 2004, pp. 632–5. (<https://doi.org/10.1109/ISBI.2004.1398617>).
- [23] L. Li, et al., Co-registration of ex vivo surgical histopathology and in vivo T2 weighted MRI of the prostate via multi-scale spectral embedding representation, *Sci. Rep.* 7 (2017) 8717.
- [24] A. Fedorov, M.G. Vangel, C.M. Tempany, F.M. Fennessy, Multiparametric magnetic resonance imaging of the prostate: repeatability of volume and apparent diffusion coefficient quantification, *Invest. Radiol.* 52 (2017) 538–546.
- [25] R. Shiradkar, et al., T1 and T2 MR fingerprinting measurements of prostate cancer and prostatitis correlate with deep learning–derived estimates of epithelium, lumen, and stromal composition on corresponding whole mount histopathology, *Eur. Radiol.* 31 (2021) 1336–1346.
- [26] RadiAnt DICOM Viewer. (<https://www.radiantviewer.com/>).
- [27] J.G. Sled, A.P. Zijdenbos, A.C. Evans, A nonparametric method for automatic correction of intensity nonuniformity in MRI data, *IEEE Trans. Med. Imaging* 17 (1998) 87–97.
- [28] J. Juntu, J. Sijbers, D. Van Dyck, J. Gielen, Bias field correction for MRI images, in: M. Kurzyński, E. Puchała, M. Woźniak, A. Żołnierczyk (Eds.), *Computer Recognition Systems*, (Springer Berlin Heidelberg, 2005, pp. 543–551.
- [29] I. Fogel, D. Sagi, Gabor filters as texture discriminator, *Biol. Cybern.* 61 (1989) 103–113.
- [30] K.I. Laws, *Textured Image Segmentation*, 1980. (<https://apps.dtic.mil/docs/citations/ADA083283>).
- [31] R.M. Haralick, K. Shanmugam, I. Dinstein, Textural features for image classification, *IEEE Trans. Syst. Man Cybern.* SMC-3 (1973) 610–621.
- [32] P. Prasanna, P. Tiwari, A. Madabhushi, Co-occurrence of local anisotropic gradient orientations (CoLLAGE): a new radiomics descriptor, *Sci. Rep.* 6 (2016) 37241.
- [33] R. Tibshirani, The Lasso method for variable selection in the cox model, *Stat. Med.* 16 (1997) 385–395.
- [34] O. Ronneberger, P. Fischer, T. Brox, U-Net: Convolutional Networks for Biomedical Image Segmentation, 2015. ArXiv150504597 Cs.
- [35] J.H. McDonald. *Handbook of Biological Statistics* 2, Parky House Publ., Baltim. MD, 2009, p. 317.
- [36] K.J. Park, S.H. Choi, J.S. Lee, J.K. Kim, M.-H. Kim, Interreader agreement with prostate imaging reporting and data system version 2 for prostate cancer detection: a systematic review and meta-analysis, *J. Urol.* 204 (2020) 661–670.
- [37] M.L. McHugh, Interrater reliability: the kappa statistic, *Biochem. Med.* 22 (2012) 276–282.
- [38] P. Schelb, et al., Classification of cancer at prostate MRI: deep learning versus clinical PI-RADS assessment, *Radiology* 293 (2019) 607–617.
- [39] P.J. van Houdt, et al., Histopathological features of MRI-invisible regions of prostate cancer lesions, *J. Magn. Reson. Imaging* 51 (2020) 1235–1246.
- [40] W.J. Catalona, et al., Selection of optimal prostate specific antigen cutoffs for early detection of prostate cancer: receiver operating characteristic curves, *J. Urol.* 152 (1994) 2037–2042.
- [41] R. Cuocolo, et al., Clinically significant prostate cancer detection on MRI: a radiomic shape features study, *Eur. J. Radiol.* 116 (2019) 144–149.
- [42] S. Bernatz, et al., Comparison of machine learning algorithms to predict clinically significant prostate cancer of the peripheral zone with multiparametric MRI using clinical assessment categories and radiomic features, *Eur. Radiol.* 30 (2020) 6757–6769.
- [43] A. Roge, et al., Evaluating the sensitivity of deep learning to inter-reader variations in lesion delineations on bi-parametric MRI in identifying clinically significant prostate cancer, in: *Medical Imaging 2022: Computer-Aided Diagnosis* 12033, SPIE, 2022, pp. 250–259.